Sizing of Multiple Cracks Using Magnetic Flux Leakage Measurements

Maryam Ravan[1], Reza K. Amineh[1], Slawomir Koziel[2], Natalia K. Nikolova[1], and James P. Reilly[1]

[1]Department of Electrical and Computer Engineering, McMaster University, Canada
[2]School of Science and Engineering, Reykjavik University, Iceland.

***Abstract*—This paper presents an approach to estimate the characteristics of multiple narrow-opening cracks from magnetic- flux-leakage signals. The number, locations, orientations and lengths of the cracks are the objective of the inversion process. The proposed procedure provides a reliable estimation of crack parameters in two separate consecutive steps. In the first step, the Canny edge detection algorithm is used to estimate the number, locations, orientations and lengths of the cracks. Then, an inversion procedure based on space mapping (SM) is used in order to estimate the crack depths efficiently. The accuracy of the proposed algorithm is examined via simulations based on the finite element method (FEM) as well as real experimental MFL data.**

***Index Terms*— multiple cracks, sizing, magnetic flux leakage (MFL), edge detection, space mapping optimization.**

1. Introduction

Magnetic-flux-leakage (MFL) technique is often used for in-service inspection of the structural integrity of ferromagnetic structures. This technique has been used to locate and assess defects such as fatigue cracks, corrosion, erosion and abrasive wear. In most practical cases, the MFL technique is used to measure cracks having widths of a few millimeters. Sizing of cracks is an important task in the safety inspection and the maintenance of various industrial structural components.

The MFL inversion techniques often use an iterative approach where a forward problem is solved in a feedback loop to reconstruct crack parameters. The forward problem is often solved with one of the following approaches: numerical models such as the finite element method (FEM) (*e.g.*, [1]-[3]), analytical models (*e.g.*, [4]–[7]) and neural networks (*e.g.*, [8]–[12]). Numerical models provide accurate results but they are computationally expensive while analytical models and neural networks are fast but less accurate due to the approximations made in deriving these models.

To take the advantage of the speed of the analytical formulas and the accuracy of the FEM, the space mapping (SM) optimization method [13]-[18] has been applied as an efficient tool in single crack parameter estimation from FEM simulated MFL signals [19]. In that work, it is assumed that the crack has a predetermined location and orientation and the crack length

and depth are estimated using the SM algorithm. However, in practical situations, cracks usually occur in clusters with unknown location and orientation.

There are some methods to extract multiple-crack parameters from MFL signals (*e.g.*, [20]-[22]) but these methods deal with predetermined arrangements of cracks, which reduces their applicability in practice. Dealing with multiple cracks under practical conditions, *i.e.*, without any *a priori* knowledge, requires the optimization of a large number of parameters. This often results in deterministic optimization procedures being trapped in local minima. On the other hand, stochastic methods such as genetic algorithms and simulated annealing, which have the ability of finding the global minimum, are computationally expensive.

In this paper we extend the previous work [19] by proposing a novel two-step optimization procedure so that an arbitrary arrangement of multiple cracks can be analyzed. In the first step, we estimate the number of cracks and their locations, orientations and lengths by applying an edge detection algorithm directly to the MFL signal. Then, we estimate the depth of each crack by using the SM optimization procedure. The efficiency and speed of the proposed algorithm is validated with the reconstruction of the crack parameters from simulated and measured MFL signals.

The rest of the paper is organized as follows. Section 2 describes the estimation of the parameters of the crack opening such as their number, locations, orientations, and lengths. Then the analytical formulas and the FEM, used as forward models in the SM optimization, are explained in Sections 3 and 4, respectively. Section 5 briefly describes the SM algorithm. The crack geometry estimation method is then proposed in Section 6 to estimate crack parameters by combining the methods in Sections 2 and 5. To validate the efficiency of the inversion method proposed in this paper, the results of several case studies are discussed in Section 7.

2. Estimation of the Crack Opening Parameters

The MFL technique relies on the fact that when a magnetic field is applied to a ferromagnetic material, any discontinuity and/or local gradients in the magnetic permeability in the test material cause variations of the leakage field. This flux leakage is measured by a magnetic field sensor and is used to estimate the dimensions of the defect.

The positions of the peaks in the spatial gradient of the 2-D measured magnetic field give a proper approximation of the location, orientation and length of each crack [23]. This allows for proper edge detection with the measured signal and consequently the extraction of these parameters. Here, we employ the Canny edge detection algorithm [24]. The Canny edge detector first smoothes an image by convolution with a Gaussian mask to eliminate most of the noise. Next, the algorithm attempts to detect edges through the maxima of the gradient modulus. This algorithm produces an edge strength and direction at each pixel in the smoothed image. The computations are based on determining the gradient magnitude as the root of the sum of the squares of the derivatives in both directions x and y. The direction of the edge is computed using the arctan of the derivative

ratios. Thus the algorithm is based on three parameters: σ , which is the standard deviation of the Gaussian mask, T_{low} and T_{high} , which are used for thresholding to determine if a pixel belongs to an edge or not.

3. Analytical model to predict the MFL response

In analytical approaches, the magnetic flux leakage is formulated mathematically by a dipole model [4]–[7]. The crack is represented as being filled by magnetic dipoles all oriented against the direction of the applied magnetic field. These magnetic dipoles generate a magnetic field outside the metal, which is equivalent to a leakage magnetic field. A surface crack is illustrated in Fig. 1. It has nonzero orientation θ from the positive *x*-axis in a clockwise direction, length 2*l* (along the ρ -axis), width 2*a* (perpendicular to the ρ -axis), and depth *d* (along the *z*-axis).

The magnetic field $d\mathbf{H}$ generated at a distance $\boldsymbol{r}$ by the element of charge, $dp = \sigma_s \, d\rho \, dz'$, is given by [4]

$$d\mathbf{H}(x, y, z) = \frac{dp}{4\pi r^3} \cdot \boldsymbol{r} = \frac{\sigma_s d\rho dz'}{4\pi r^3} . \boldsymbol{r} \tag{1}$$

By integrating (1) over the surface of the defect wall, the *y*-component of the magnetic field at a point with coordinates *x*, *y*, *z* is given by

$$H_y(x, y, z) = \frac{\sigma_s}{4\pi} \left(\int_{-d}^{0} \int_{-l}^{l} \frac{(y - \rho \sin\theta + a\cos\theta)\, d\rho\, dz'}{r_+^3} - \int_{-d}^{0} \int_{-l}^{l} \frac{(y - \rho \sin\theta - a\cos\theta)\, d\rho\, dz'}{r_-^3} \right) \tag{2}$$

where $r_+ = [(x - \rho\cos\theta - a\sin\theta)^2 + (y - \rho\sin\theta + a\cos\theta)^2 + (z - z')^2]^{1/2}$ and $r_- = [(x - \rho\cos\theta + a\sin\theta)^2 + (y - \rho\sin\theta - a\cos\theta)^2 + (z - z')^2]^{1/2}$. After computing the magnetic field of each crack, the total magnetic field is calculated as a simple superposition of the magnetic fields of the separate cracks.

This model assumes that each rectangular crack is filled homogeneously by magnetic dipoles, *i.e.*, the surface density of the magnetic charge has constant value on both walls of the rectangular crack. This assumption can lead to significant error in calculating the magnetic field in the vicinity of each crack because the distribution of the magnetic dipoles along the crack depth is in fact not constant [7]. Also, this model does not consider the mutual influence of neighboring cracks. This may affect the accuracy of the calculated magnetic field when the cracks are close to each other [5]. Although considering these effects may produce more accurate results in some special cases (*e.g.* [5], [7]), they increase the computational complexity and are not general. Here, since we use the analytical model as a fast and less accurate 'coarse' model, we can afford the simplicity of the model assuming constant distribution of the magnetic dipole density and neglecting the effect of mutual influence among the cracks.

4. FEM Simulations to Predict MFL Response

The MFL problem can be treated as a magnetostatic problem, which can be formulated as [25]

$$\nabla \times \nabla \times \mathbf{A} = \mu_0 (\mathbf{J} + \nabla \times \mathbf{M}) \tag{3}$$

where μ_0, **J** and **A** are the permeability of vacuum, the current density and the magnetic vector potential, respectively. The magnetization **M** is a non-linear function of $\mathbf{B} = \nabla \times \mathbf{A}$. The nonlinear equation (3) is solved iteratively.

A nonlinear FEM using Maxwell v. 11 [26] is used for simulating the three-dimensional (3-D) magnetic field around and inside a surface defect in a steel slab. Fig. 1 shows the model geometry. Steel_1010 is selected from the simulator's library as the material type for the steel slab.

In order to decrease the computational time and still maintain good accuracy, a simplified model of the magnetizer is used. The steel slab is magnetized with two parallel magnets (Fig. 1). NDFe35 is selected as the magnet material. It magnetizes the steel plate in the *y*-direction with a coercivity such that the operating point is in the knee of the B-H curve for Steel_1010. This is desirable because it leads to the maximum signal-to-noise ratio for obtaining the leakage crack signal [25].

The boundary conditions are set so that to enforce the magnetic field inside the metal to be parallel to the *y*-axis. They are: (a) zero normal component of the magnetic field to all faces of the magnetizers except the faces which are parallel to the *x*-*z* plane; (b) zero tangential components of the magnetic field at the faces of the magnetizers which are parallel to the *x*-*z* plane; (c) zero normal component of the magnetic field at the faces of the steel which are parallel to the *y*-*z* plane.

5. Space Mapping Optimization

The space mapping (SM) technique shifts the optimization burden from an expensive 'fine' (or high-fidelity) model $\boldsymbol{R}_f(\boldsymbol{x}_f)$: $R^n \to R^m$ to a cheap 'coarse' (or low-fidelity) model $\boldsymbol{R}_c(\boldsymbol{x}_c)$: $R^n \to R^m$ by iterative optimization and updating of the surrogate model $\boldsymbol{R}_s(\boldsymbol{x}_c)$ which is built using the coarse model and available fine model data:

$$\boldsymbol{R}_s(\boldsymbol{x}_c) = \boldsymbol{R}_c(p(\boldsymbol{x}_f)) \approx \boldsymbol{R}_f(\boldsymbol{x}_f). \tag{4}$$

A variety of SM surrogate models is available [17], [18]. One of the most popular approaches is the so-called input SM [13], in which the mapping function *p*: $R^n \to R^n$, relating the fine and coarse model variables is defined as

$$p(\boldsymbol{x}_f) = \boldsymbol{B} \cdot \boldsymbol{x}_f + \boldsymbol{c} \tag{5}$$

Here, we set $\boldsymbol{B}$=1 and use the shift-based input space mapping with only parameter $\boldsymbol{c}$. This particular model has been chosen because it is simple and yet it provides sufficient matching with the fine model. The SM optimization algorithm used in this paper is summarized in the following steps.

Step 1) Choose the analytical model described in Section 3 (implemented in Matlab [27]) as the coarse model.

Step 2) Choose the FEM simulation described in Section 4 ((implemented in Maxwell v. 11 [26]) as the fine model.

Step 3) Set $\boldsymbol{x}_f = \{x_1, x_2, ..., x_N\}$ as the crack depths vector

Step 4) Use the SM technique to find the mapping p and the fine model parameters, $\boldsymbol{x}_f$ which are iteratively updated until the termination condition is satisfied [19].

6. Crack Geometry Estimation

The overall approach to solve the inverse problem in this paper can be outlined as follows. A color map of the 2-D measured signal is generated and treated as an image. The Canny edge detection algorithm is then applied to this image to extract the edge of crack openings [24]. The edges of crack openings can give us information about the number, locations, orientations and lengths of the cracks. This information is then used to analyze the problem in the coarse and fine models of the SM optimization algorithm for the estimation of the crack depths. We use the SMF system [28] to perform the SM optimization.

The termination condition for the SM algorithm is

$$\frac{\| \boldsymbol{x}^{(i+1)} - \boldsymbol{x}^{(i)} \|}{\| \boldsymbol{x}^{(i)} \|} \leq \delta \tag{6}$$

where $\| \cdot \|$ is the l_2-norm, $\boldsymbol{x}^{(i)}$, i = 0, 1, …, is the sequence of solutions produced by the SM algorithm and $0 < \delta \ll 1$ is a user defined constant.

7. Results

Results of various simulation and measurement tests are presented here to assess the accuracy and the computational efficiency of the proposed inversion technique. First we present the simulated results of three different arrangements of multiple cracks as shown in Fig.2. The thickness of the steel slab is 5.6 mm. Table 1 shows the parameter values of these cracks. The target MFL responses for three cases are the *y*-component distributions of the magnetic field calculated at the surface of the metal using FEM simulations. We assume that the length and depth of each rectangular crack lie between two limiting values as

$$5 \text{ mm} \leq l \leq 65 \text{ mm} \tag{7 (a)}$$

$$0.5 \text{ mm} \leq d \leq 5 \text{ mm} . \tag{7 (b)}$$

The performance of the SM algorithm depends on the similarity between the fine model and the coarse model, which can be expressed in rigorous mathematical terms (*e.g.*, [18]). In our case, because the maximum amplitudes of the MFL distributions obtained from the coarse and fine models are substantially different, we use the scaling surface applied in [19] to align them.

The scaling surface is provided for the case where the orientation of the crack is perpendicular to the external applied field ($\theta = 0^\circ$). However, when the crack has any other orientation ($\theta \neq 0^\circ$), we can find the projection of the applied magnetic field

Table 1

Length, Orientation and Depth for the Rectangular Cracks

Crack name	Length, l (mm)	Orientation, θ (degree)	Depth, d (mm)
Crack1 (Fig. 2(a))	20	135	1.6
Crack2 (Fig. 2(a))	30	125	2.3
Crack3 (Fig. 2(a))	45	73	3.2
Crack4 (Fig. 2(a))	65	62	4.4
Crack1 (Fig. 2(b))	10	10	1.0
Crack2 (Fig. 2(b))	35	150	2.5
Crack3 (Fig. 2(b))	50	20	3.4
Crack1(Fig. 2(c))	16	40	1.8
Crack2(Fig. 2(c))	35	35	3.6
Crack3(Fig. 2(c))	40	25	4.7
Crack4(Fig. 2(c))	24	24	2.1

H_0 on an axis perpendicular to the crack as [23] , [29]:

$$H_0' = H_0 \cos\theta . \tag{8}$$

Thus, the scaling surface constructed for cracks with $\theta \neq 0^\circ$ is corrected using the factor $\cos\theta$.

The total leakage field at a point above the metal is then approximated by a sum of the scaled leakage fields of the corresponding set of rectangular cracks

$$H_y(x,y,z) = \sum_{i=1}^{N} M_i \cos\theta_i \cdot H_{y_i}(x,y,z) \tag{9}$$

where M_i is the scaling factor for the *i*th rectangular crack calculated in [19], θ_i is its orientation angle and $H_{y_i}(x,y,z)$ is the *y*-component of the magnetic field for the *i*th rectangular crack calculated from (2). The SM optimization described in Section 5 is used to estimate the crack depth parameters. We use the termination condition (6) with δ equal to 0.001.

Figs. 3(a) , 4(a) and 5(a) show the color map of the 2-D MFL signal (H_y) for three arrangements of cracks. We can estimate the edge of each crack accurately by applying the Canny edge detector to this color map. Figs. 3(b), 4(b) and 5(b) show the edge of the cracks in Figs. 2(a), 2(b) and 2(c) respectively. From these edges we can easily extract accurately the number, locations, orientations and lengths of the cracks.

Figs. 3(c), 3(d), 4(c), 4(d), 5(c) and 5(d) compares the target MFL responses with MFL responses obtained using the SM optimal points, *i.e.* $\overline{\boldsymbol{x}}_f$ for all investigated cracks in Fig. 2. We use two rows of the 2-D MFL signal that passes across the cracks as target signals for the SM optimization algorithm. Tables 2 and 3 show the quantitative comparison of the proposed method, where the mean relative error (MRE) between the original crack parameter and its reconstruction counterpart is given. MRE is defined as

$$\mathrm{MRE}(\hat{q}) = \frac{|q-\hat{q}|}{q} \times 100 \tag{10}$$

where q and $\hat{q}$ denote the actual and solution points (l, θ or d) respectively. These results show that the Canny method can detect the edge of the crack opening precisely and then the SM algorithm can estimate the depth accurately for orientations in the ranges from $0 \le \theta \le 70^\circ$ and $110^\circ \le \theta \le 180^\circ$. For orientations in the range of $70^\circ \le \theta \le 110^\circ$ (crack3 in Fig. 2(a)), the strength of the signal and consequently the signal to noise ratio (SNR) are not large enough which causes loss of accuracy in the crack parameter estimation. Also, in the case where the cracks are close to each other (Fig. 2(c)), the MFL signals of deeper cracks affect the MFL signal of shallower cracks that causes higher MRE of the depth estimation for the shallower cracks (crack1 and crack4 in Fig. 2(c)).

The SM optimization converges after few fine model evaluations (8 and 7 and 5 evaluations for crack arrangements in Fig. 2(a), 2(b) and 2(c), respectively). In order to confirm the efficiency of the SM optimization in getting fast and accurate results, Table 3 also compares the results with direct optimization of the fine model. We choose 1 mm depth as the initial points for all cracks in Fig. 2. The solutions via direct optimization of the fine model using sequential quadratic programming (SQP) converges after 108, 91 and 76 fine model evaluations for crack arrangements in Figs. 2(a), 2(b) and 2(c), respectively. It should be noted that a single FEM simulation takes about 10 minutes of CPU time using an Intel Core 2 Duo processor at 2.4 GHz. This means that the direct optimization of the fine model requires in excess of 12 hours of CPU time while SM optimization requires only about 1:10 hours on average. Thus the direct optimization of the fine model is far more computationally expensive than SM optimization.

The solutions found for the direct optimization with the termination condition of (6) with $\delta = 0.001$ and their corresponding values of MRE are shown in Table 3. These large errors demonstrate that in all cases the direct optimization leads to local minima, which are not the best solutions available. In contrast, SM optimization converges to the true solutions with the final result having much smaller MRE.

To further examine the accuracy of the proposed method, we present two measured results from a real MFL inspection for two single cracks [23]. The cracks are fabricated using electric discharge machine (EDM) technique. They share the same opening width ($2a$ = 0.1 mm) and orientation ($\theta = 0^\circ$) but have different lengths of l = 25 mm and l = 50 mm and different depths of d = 3.3 mm and d = 2.2 mm. Figs. 6 and 7 show the 3-D plot and 2- D color map of the measured signals for the two cracks and their corresponding edge detection and SM optimization results. Here, we should mention that the detection area of the Hall sensor is 3 mm $\times$ 4 mm. This area restricts the resolution of the measured set up to the dimension of the sensor. Thus, in the case of narrow-opening crack, the distance between the two detected edges of the opening increases to the sampling rate of the sensor. When the two detected edges of the defect are closer to each other than the sensor resolution, the defect is treated as a crack that is placed in the middle between the two detected edges. Also, the area of the Hall sensor has a low-pass filtering

Table 2
Length and orientation Results of Canny Edge detection algorithm for Investigated Cracks.

Crack name	Estimated length ($\hat{l}$)	MRE for $\hat{l}$	Estimated orientation ($\hat{\theta}$)	MRE for $\hat{\theta}$
Crack1 (Fig. 2(a))	21.07	5.3500	136.15	0.8519
Crack2 (Fig. 2(a))	30.13	0.4333	125.27	0.2160
Crack3 (Fig. 2(a))	43.62	3.0667	74.6	2.1918
Crack4 (Fig. 2(a))	66.2	1.8462	61.5	0.8065
Crack1 (Fig. 2(b))	9.92	0.8000	9.27	7.3000
Crack2 (Fig. 2(b))	35.13	0.3714	150.7	0.4667
Crack3 (Fig. 2(b))	50.54	1.0800	19.65	1.7500
Crack1(Fig. 2(c))	15.62	2.37	39.80	0.50
Crack2(Fig. 2(c))	35.62	1.74	34.59	1.17
Crack3(Fig. 2(c))	38.51	3.72	23.19	7.24
Crack4(Fig. 2(c))	23.71	1.21	24.94	3.92

Table 3
Depth Estimation Results of SM Optimization for Investigated Cracks.

Crack name	Estimated depth ($\hat{d}$) (SM optimization)	MRE for $\hat{d}$	Estimated depth ($\hat{d}$) (direct optimization)	MRE for $\hat{d}$
Crack1 (Fig. 2(a))	1.63	1.87	0.72	55
Crack2 (Fig. 2(a))	2.31	0.43	1.67	27.4
Crack3 (Fig. 2(a))	2.82	11.87	2.53	20.9
Crack4 (Fig. 2(a))	4.35	1.14	4.5	2.27
Crack1 (Fig. 2(b))	0.97	3.00	0.5	50
Crack2 (Fig. 2(b))	2.51	0.40	3.12	24.8
Crack3 (Fig. 2(b))	3.47	2.06	3.23	5
Crack1(Fig. 2(c))	1.62	10.00	1.10	38.89
Crack2(Fig. 2(c))	3.58	0.56	3.33	7.50
Crack3(Fig. 2(c))	4.68	0.42	5.00	6.38
Crack4(Fig. 2(c))	1.81	13.81	1.63	22.38

effect on the MFL signal that increases the error in length estimation, especially in the case of shorter cracks.

When working with measured signals, in order to align the maximum amplitudes of the measured signal to the FEM simulated signal, we use another scaling surface. We construct this surface using measurement and simulation results for a sample set of nine artificially manufactured cracks and defined four quadrant sub-surfaces [23]. Each sub-surface element is described by four cracks using linear inter/extrapolation. The length estimated from the Canny method together with a scaled version of the measured signal is used to set the scale of the SM optimization algorithm for depth estimation. Tables 4 and 5 summarize the results for the length and depth estimation of the two measured cracks using the proposed method and the method in [23]. A comparison of the results demonstrates that the two methods estimate the crack length with the same accuracy. This is due to the fact that the method for length estimation in [23] is a special 1-D case of the Canny gradient method. However, the proposed algorithm can estimate the crack depth more accurately. Notice that the more general Canny algorithm eliminates the need to estimate the orientation angle θ of the crack in a separate step as done in [23].

Table 4
Estimation of Length and Depth Using the Proposed Method.

Crack parameters (mm)	$\hat{l}$ (mm) (Canny method)	MRE for $\hat{l}$	$\hat{d}$ (mm) (SM optimization)	MRE for $\hat{d}$
l=25, d=3.3	32	28	3.14	4.85
l=50, d=2.2	62	24	2.33	5.91

Table 5
Estimation of Length and Depth Using the Method in [23].

Crack parameters (mm)	$\hat{l}$ (mm) (Method in [23])	MRE for $\hat{l}$	$\hat{d}$ (mm) (Method in [23])	MRE for $\hat{d}$
l=25, d=3.3	32	28	2.42	26.67
l=50, d=2.2	62	24	1.85	15.91

8. Conclusion

An inversion method has been proposed for estimating the number, locations, orientations, lengths and depths of multiple cracks with arbitrary arrangements from MFL signals. The method employs the Canny edge detection algorithm to detect simultaneously the number, locations, orientations and lengths of cracks and the SM optimization algorithms to estimate the crack depths. The proposed methodology was tested and verified for three different arrangements of simulated rectangular cracks. The results demonstrated that the Canny edge detector can precisely detect the length and orientation of each crack and is useful to reduce the number of optimizable parameters in the SM optimization, which leads to improved inversion results. Also, the results show that the SM inversion technique can estimate the depth of the crack more accurately than the direct fine model optimization while there is a dramatic reduction in the number of fine model evaluations and therefore CPU time. To examine the accuracy of the proposed method in practice, we then test it with measured results of two fabricated single cracks. The results demonstrate that the proposed method can estimate the crack depth more accurately than the direct method in [23]. It was noticed that the area of the Hall sensor affects the accuracy of the length estimation. The proposed methodology based on the Canny edge detection and SM optimization can be applied to arbitrary shape defects as well. However, a more general coarse model is needed to enable the SM optimization in this case. This important development is the subject of another work.

References

[1] Schifini, R. and Bruno, A. C.: ‘Experimental verification of a finite element model used in a magnetic flux leakage inverse problem’, J. Phys. D: Appl. Phys., 2005, 38, (12), pp. 1875-1880

[2] Chen, Z., Preda, G., Mihalache, O., and Miya, K.: ‘Reconstruction of crack shapes from the MFLT signals by using a rapid forward solver and an optimization approach’, IEEE Trans. Magn., 2002, 38, (2), pp. 1025-1028

[3] Yan, M., Udpa, S., Mandayam, S., Sun, Y., Sacks, P., and Lord, W.: 'Solution of inverse problems in electromagnetic NDE using finite element methods', IEEE Trans. Magn., 1998, 34, (5), pp. 2924-2927

[4] Edwards, C., and Palmer, S. B., 'The magnetic leakage field of surface-breaking cracks', J. Phys. D: Appl. Phys., 1986, 19, (4), pp 657-673

[5] Zagidulin, R. V., Muzhitskii, V. F., and Bizyulev, A. N.: 'Effect of the number of surface flaws in a group on their magnetic field', Russian J. of NDT, 2004, 40, (8), pp. 507–511

[6] Zagidulin, R. V., Muzhitskii, V. F., and Kurozaev, V. P.: 'Resolution of discontinuity flaws based on measurements of magnetic field configuration', Russian J. of NDT, 2000, 36, (5), pp. 344-352

[7] Minkov, D., Lee, J., and Shoji, T.: 'Study of crack inversions utilizing dipole model of a crack and Hall element measurements', J. Magn. Magn. Mater, 2000, 217, (1), pp. 207–215

[8] Ramuhalli, P., Udpa, L., and Udpa, S. S.: 'Electromagnetic NDE signal inversion by function-approximation neural networks,' IEEE Trans. Magn., 2002, 38, (6), pp. 3633-3642

[9] Han, W. and Que, P.: '2-D defect reconstruction from MFL signals by a genetic optimization algorithm', Russian J. of NDT, 2005, 41, (12), pp. 809–814

[10] Han, W. and Que, P.: 'Defect reconstruction of submarine oil pipeline from MFL signals using genetic simulated annealing algorithm', J. Japan Petr. Inst., 2006, 49, (3), pp. 145-150

[11] Ramuhalli, P., Udpa, L., and Udpa, S. S.: 'Neural network-based inversion algorithms in magnetic flux leakage nondestructive evaluation', J. Appl. Phys., 2003, 93, (10), pp. 8274–8276

[12] Joshi, A., Udpa, L., Udpa, S. S., and Tamburrino, A.: 'Adaptive wavelets for characterizing magnetic flux leakage signals from pipeline inspection', IEEE Trans. Magn., 2006, 42, (10) , pp. 3168-3170

[13] Bandler, J. W., Biernacki, R. M., Chen, S. H., Grobelny, P. A., and Hemmers, R. H.: 'Space mapping technique for electromagnetic optimization', IEEE Trans. Microw. Theory Tech., 1994, 2, (12), pp. 2536–2544

[14] Bandler, J. W., Cheng, Q. S., Gebre-Mariam, D. H., Madsen, K., Pedersen, F., and Søndergaard, J.: 'EM-based surrogate modeling and design exploiting implicit, frequency and output space mappings', IEEE MTT-S Int. Microw. Symp. Dig., Philadelphia, PA, , June 2003, pp. 1003–1006

[15] Bandler, J. W., Cheng, Q. S., Dakroury, S. A., Mohamed, A. S., Bakr, M. H., Madsen, K., and Søndergaard, J.: 'Space mapping: The state of the art', IEEE Trans. Microw. Theory Tech., 2004, 52, (1), pp. 337–361

[16] Echeverria, D. and Hemker, P.W.: 'Space mapping and defect correction', CMAM The International Mathematical Journal Computational Methods in Applied Mathematics, 2005, 5, (2), pp. 107-136

[17] Bandler, J. W., Koziel, S., and Madsen, K.: 'Space mapping for engineering optimization', SIAG/Optimization Views-and-News Special Issue on Surrogate/Derivative-free Optimization, 2006, 17, (1), pp. 19-26

[18] Koziel, S., Bandler, J. W., and Madsen, K.: 'A space-mapping framework for engineering optimization: theory and implementation', IEEE Trans. Microw. Theory Tech., 2006, 54, (10), pp. 3721–3730

[19] Amineh, R. K., Koziel, S., Nikolova, N. K., Bandler, J. W., and Reilly, J. P.: 'A space mapping methodology for defect characterization from magnetic flux leakage measurements', IEEE Trans. Magn., 2008, 44, (8) , pp. 2058- 2065

[20] Gotoh, Y. and Takahashi, N.: '3-D nonlinear eddy-current analysis of alternating magnetic flux leakage testing - analysis of one crack and two cracks', IEEE Trans. Magn., 2002, 38, (2), pp. 1209–1212

[21] Gotoh, Y. and Takahashi, N.: 'Study on problems in detecting plural cracks by alternating flux leakage testing using 3D nonlinear eddy current analysis', IEEE Trans. Magn., 2003, 39, (3), pp. 1527–1530

[22] Gotoh, Y. and Takahashi, N.: 'Proposal of detecting method of plural cracks and their depth by alternating flux leakage testing: 3-D nonlinear eddy current analysis and experiment', IEEE Trans. Magn., 2004, 40, (2), pp. 655–658

[23] Amineh, R. K., Nikolova, N. K., Reilly, J. P., and Hare, J. R.: 'Characterization of surface breaking cracks using one tangential component of magnetic leakage field', IEEE Trans. Magn., 2008,.44, (4), pp. 516–524

[24] Canny, J. F.: 'A computational approach to edge detection', IEEE Trans. Pattern Anal. Mach. Intell., 1986, 8, (6), pp. 679–698

[25] Park, G. S. and Park, E. S.: 'Improvement of the sensor system in magnetic flux leakage-type nondestructive testing (NDT)', IEEE Trans. Magn., 2002, 38, (2), pp. 1277-1280

[26] Maxwell Version 11.1.1, Ansoft Corporatin, http://www.ansoft.com, 2006.

[27] Matlab™, Version 7.1, The MathWorks, Inc., 3 Apple Hill Drive, Natick, MA 01760-2098, 2005.

[28] Koziel, S. and Bandler, J.W.: 'SMF: a user-friendly software engine for space-mapping-based engineering design optimization', Int. Symp. Signals, Systems and Electronics, August 2007, pp. 157-160

[29] Melikhov, Y., Lee, S. J., Jiles, D. C., Lopez, R., and Brasche, L.: 'Analytical approach for fast computation of magnetic flux leakage due to surface defects', Digests of the IEEE Int. Magnetics Conference (INTERMAG), April 2005, pp. 1165 - 1166

List of figure captions

Fig. 1. Dipolar representation of rectangular crack.

Fig. 2. 3-D view of three different arrangements of the multiple cracks.

Fig. 3 (a) Color maps of the 2-D MFL signal for cracks of Figs. 2(a); (b) its corresponding Canny edge detector results; (c), (d) comparison of the target MFL response with the MFL response obtained at the SM optimal point for cracks of Fig.2 (a) at x=-16mm and x=30mm respectively.

Fig. 4 (a) Color maps of the 2-D MFL signal for cracks of Figs. 2(b); (b) its corresponding Canny edge detector results; (c),(d) Comparison of the target MFL response with the MFL response obtained at the SM optimal point for cracks of Fig.2 (b) at x=0mm and x=40mm respectively.

Fig. 5 (a) Color maps of the 2-D MFL signal for cracks of Figs. 2(c); (b) its corresponding Canny edge detector results; (c),(d) comparison of the target MFL response with the MFL response obtained at the SM optimal point, for cracks of Fig.2 (c) at y=-2mm and y=6mm respectively.

Fig. 6 (a) 3-D plot and (b) 2-D color map of the normalized MFL signal for the crack with l= 25 mm and d=3.3 mm, (c) the Canny edge detector result and (d) comparison of the target MFL response with the MFL response obtained at the SM optimal point at y=10 mm.

Fig. 7 (a) 3-D plot and (b) 2-D color map of the normalized MFL signal for the crack with l= 50 mm and d=2.2 mm, (c) the Canny edge detector result and (d) comparison of the target MFL response with the MFL response obtained at the SM optimal point at y=0 mm.

Fig.1

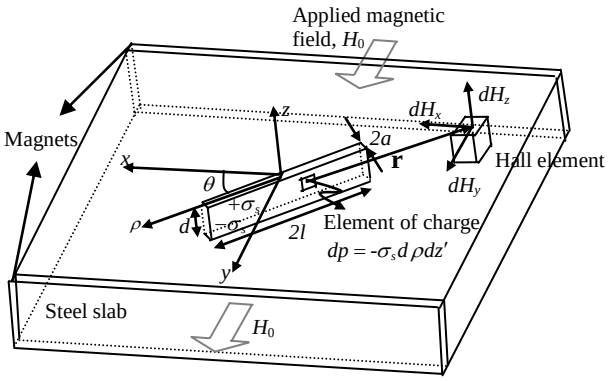

Fig.2

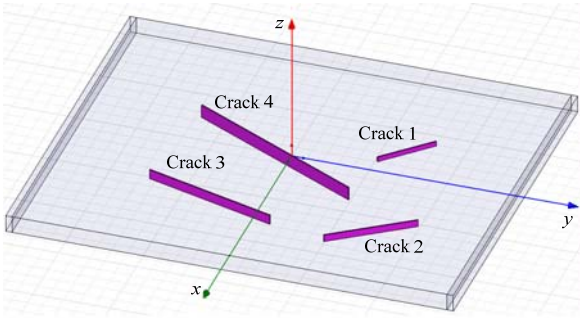

(a)

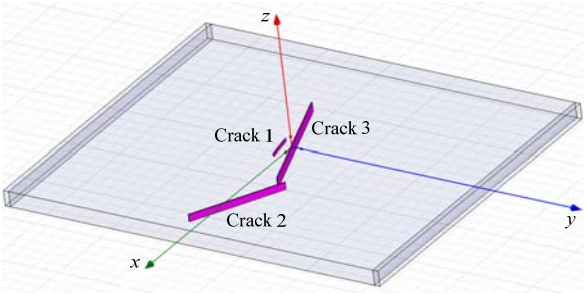

(b)

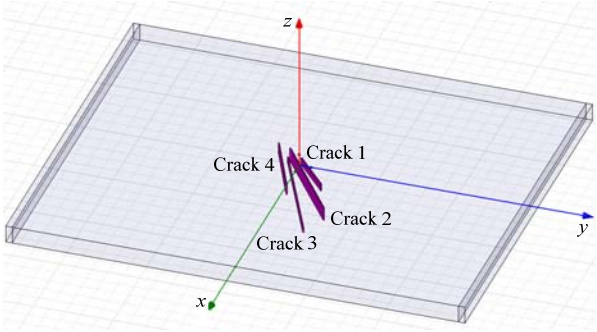

(c)

Fig.3

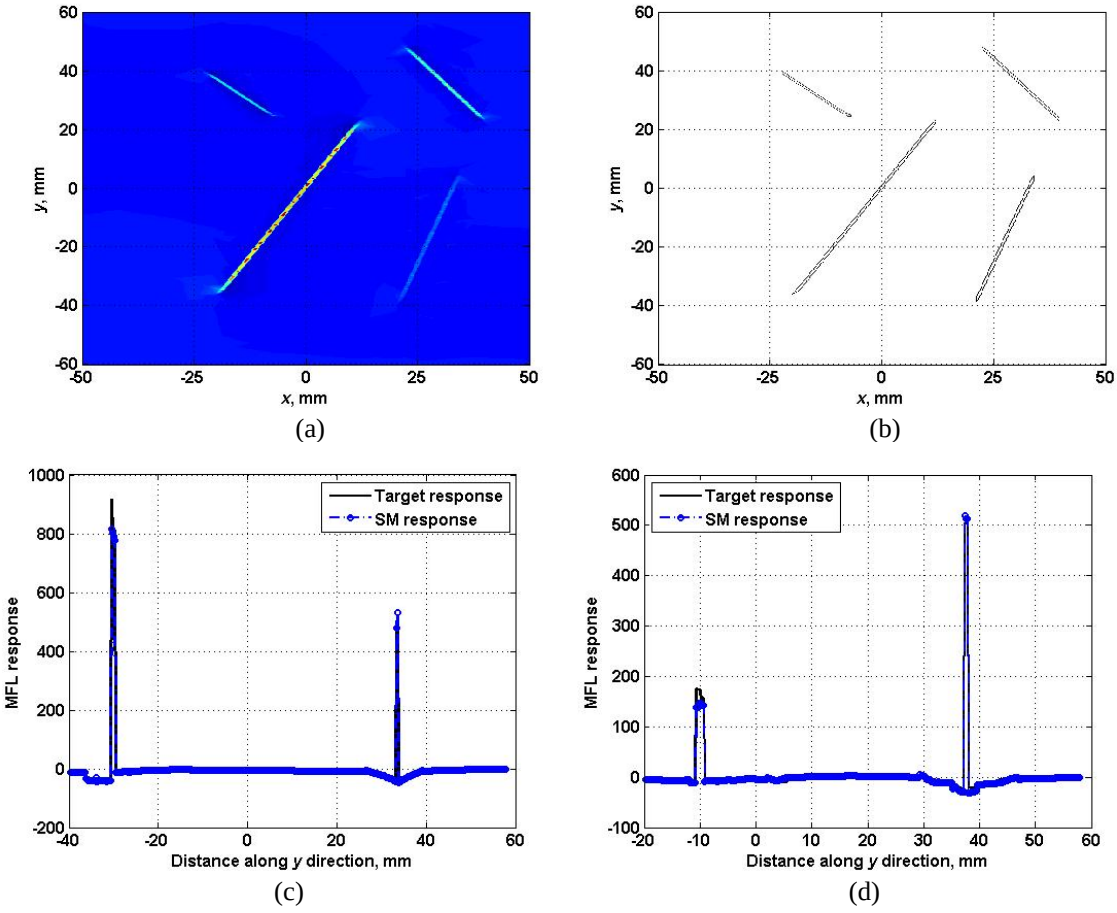
y, mm
x, mm
(a)
y, mm
x, mm
(b)
Target response
SM response
MFL response
Distance along y direction, mm
(c)
Target response
SM response
MFL response
Distance along y direction, mm
(d)

Fig. 4

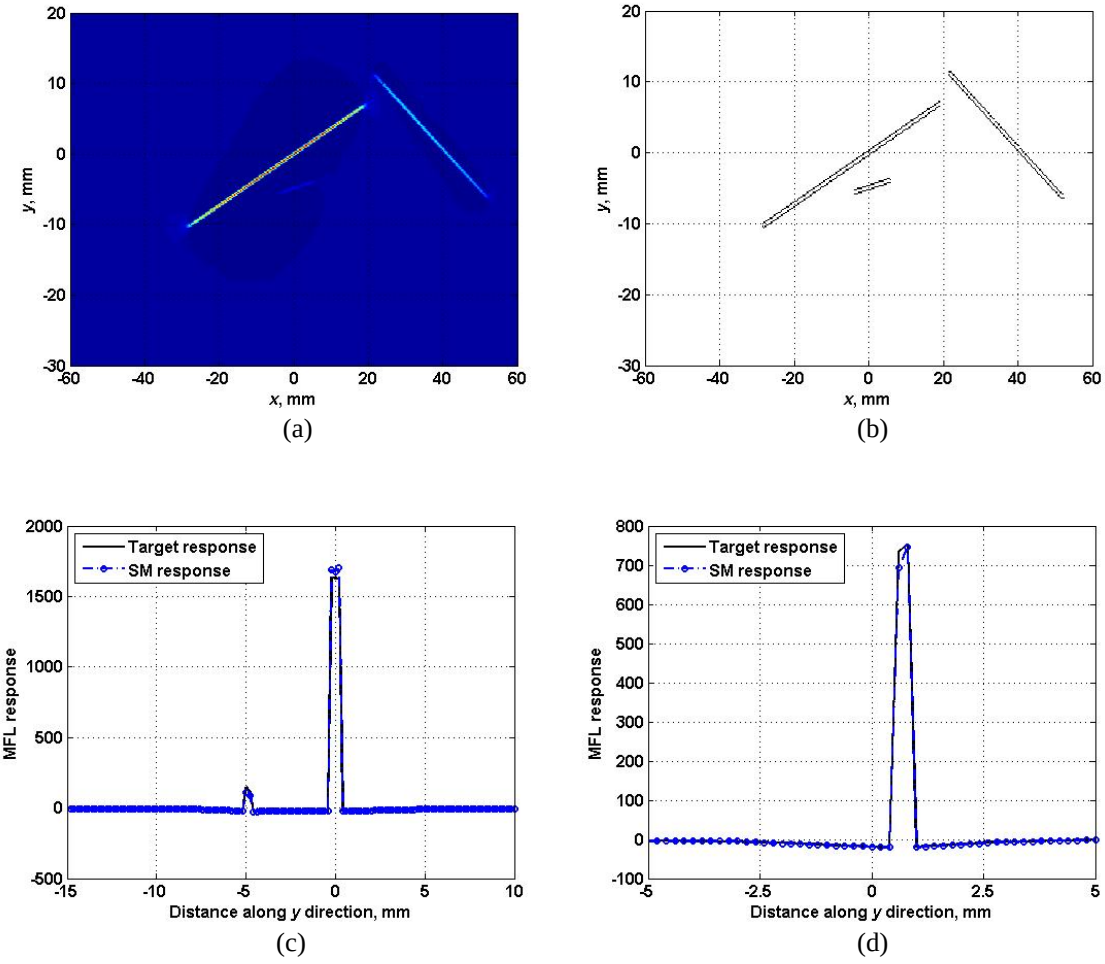
y, mm
x, mm
(a)
y, mm
x, mm
(b)
Target response
SM response
MFL response
Distance along y direction, mm
(c)
Target response
SM response
MFL response
Distance along y direction, mm
(d)

Fig.5

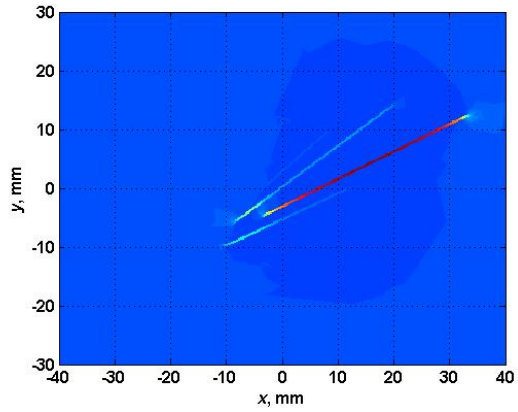
y, mm
x, mm

(a)

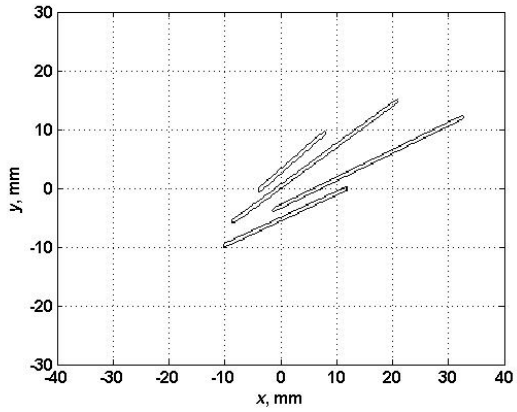
y, mm
x, mm

(b)

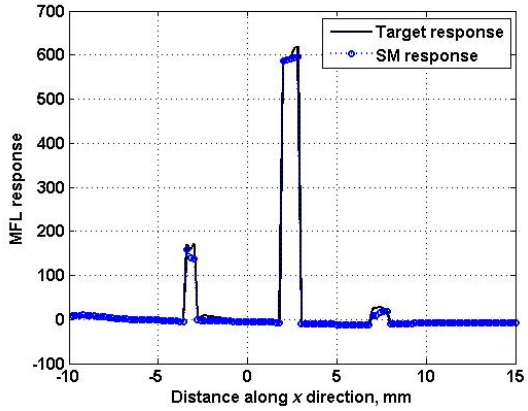
Target response
SM response
MFL response
Distance along x direction, mm

(c)

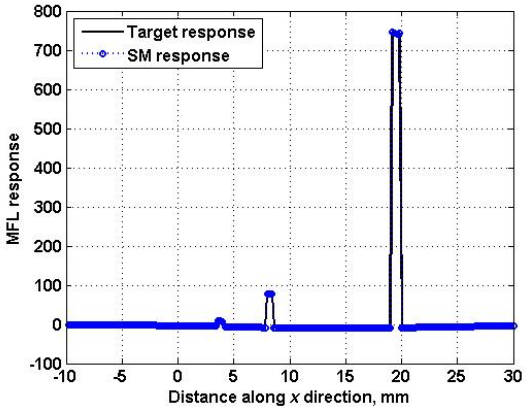
Target response
SM response
MFL response
Distance along x direction, mm

(d)

Fig.6

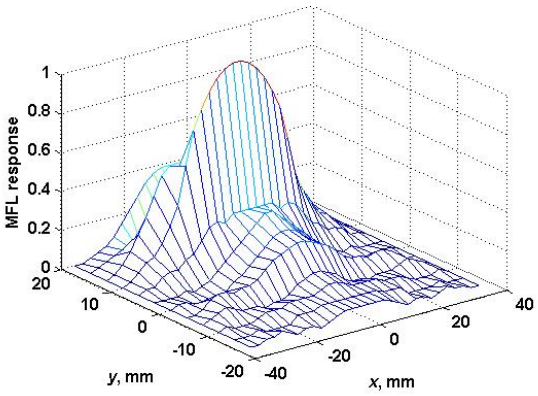
MFL response
y, mm
x, mm

(a)

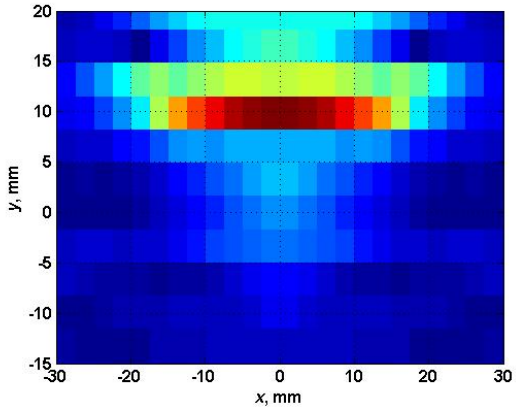
y, mm
x, mm

(b)

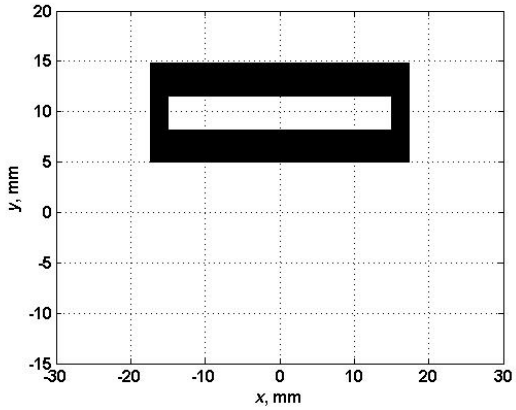
y, mm
x, mm

(c)

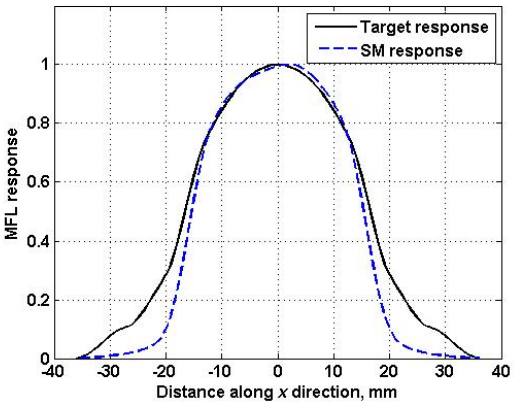
Target response
SM response
MFL response
Distance along x direction, mm

(d)

Fig.7

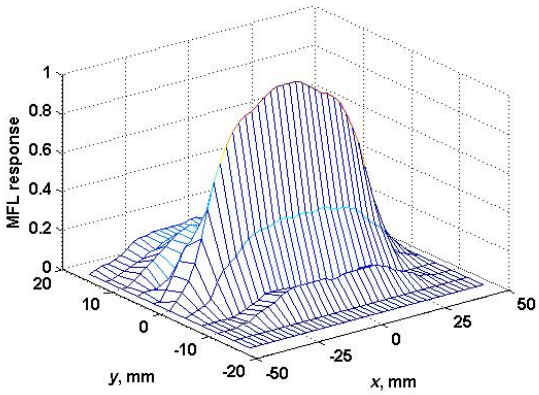
MFL response
y, mm
x, mm

(a)

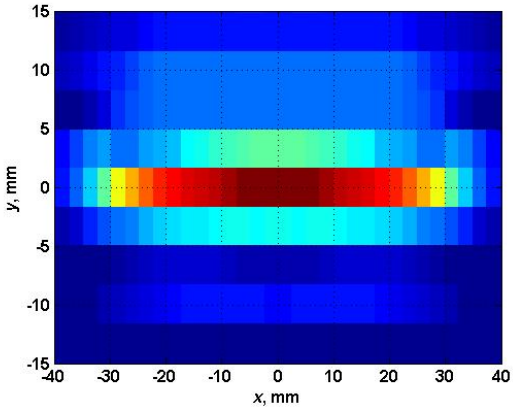
y, mm
x, mm

(b)

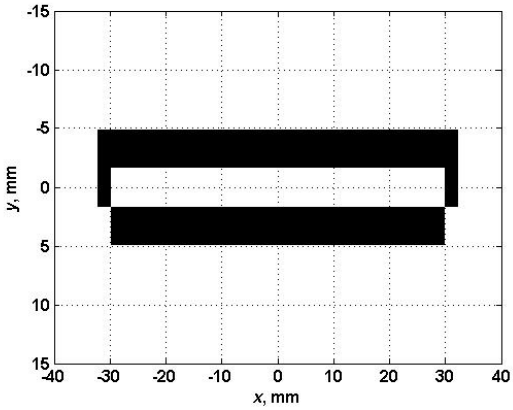
y, mm
x, mm

(c)

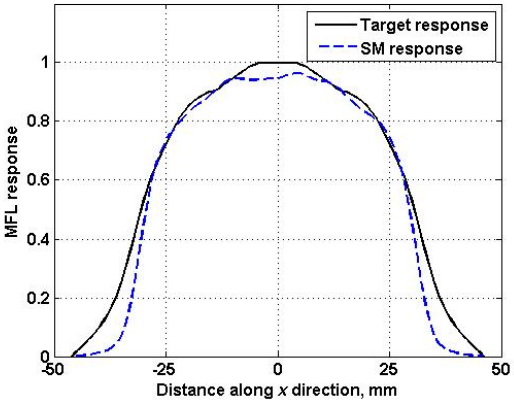
Target response
SM response
MFL response
Distance along x direction, mm

(d)